https://doi.org/10.5194/egusphere-2026-3206
Preprint. Discussion started: 30 June 2026

Summer Land-Atmosphere Coupling over Europe: A Comparative Evaluation of Observation-based Datasets

Monalisa Sahoo [1*], Stefano Materia [1,2], and Markus G. Donat [1,3]

[1]*Barcelona Supercomputing Center, Barcelona, Spain*

[2]*CMCC Foundation - Euro-Mediterranean Center on Climate Change, Bologna, Italy*

[3]*Institució Catalana de Recerca i Estudis Avançats (ICREA), Barcelona, Spain*

[*]***Corresponding author: Monalisa Sahoo****(monalisa.sahoo@bsc.es)*

https://doi.org/10.5194/egusphere-2026-3206
Preprint. Discussion started: 30 June 2026

Abstract

Land–atmosphere coupling has long been recognized to modulate the surface fluxes partitioning in transitional evaporative regimes, where soil moisture anomalies control evapotranspiration. However, globally available in-situ observations for these variables remain limited. This study provides a comprehensive assessment of the similarities, dissimilarities, and limitations among gridded observations-based datasets of surface soil moisture, evapotranspiration, potential evapotranspiration, and 2-meter air temperature across Europe. The analysis focuses on the IPCC-defined regions of Northern Europe, Eastern Europe, Western-Central Europe, and the Mediterranean during summer (June–August) for the recent 20-year period (2003–2022), and evaluates and compares the representation of land–atmosphere coupling across the different datasets. Results show that the temporal variation of the state variables and the spatial variability of land–atmosphere coupling are mostly consistent across the different datasets. On the other hand, relevant differences in absolute values and seasonal variations can be identified. Some datasets exhibit systematically distinct annual cycle patterns compared to others across variables and regions, which is also reflected in their coupling representation in both temporal and spatial structures.

Keywords: surface soil moisture, evapotranspiration, land-atmosphere coupling, summer

Short summary

This study compares several gridded observation-based datasets of soil moisture, evapotranspiration, potential evapotranspiration, and air temperature during summer across Europe from 2003–2022. It shows that datasets differ in actual values and seasonal variations, but most datasets show coherent temporal variations and coupling relationships. However, timeseries differences found for some datasets also affect their representation of land-atmosphere coupling relationships.

https://doi.org/10.5194/egusphere-2026-3206
Preprint. Discussion started: 30 June 2026

1 Introduction

Soil moisture and radiation regulate the surface fluxes through the exchange of water and energy between the soil and air. Being part of the land water and energy balance equations, evapotranspiration allows for the development and sustenance of land-atmosphere coupling processes. The coupling between land surface and atmosphere is an important modulator of climate as it influences the long-term environmental changes by affecting the precipitation, surface fluxes, evapotranspiration, and temperature. (Seneviratne et al., 2010).

Two key pathways can be identified in the land-atmosphere coupling mechanism (Dirmeyer, 2006; Ferguson et al., 2012). The land pathway is the interaction between soil moisture and surface fluxes, that becomes critical in transitional evaporative regimes where soil moisture limitation can heavily constrain evapotranspiration. The atmospheric pathway is the response of air temperature to changes in evapotranspiration. Therefore, a two-legged land-atmosphere coupling is characterized by the interaction between soil moisture and air temperature (Dirmeyer et al., 2014). In transitional evaporative regimes, these variables are negatively correlated: reductions in soil moisture lead to higher air temperatures, which in turn promote further soil drying (Fischer et al., 2007; Vautard et al., 2007; Hirschi et al., 2011; Santanello Jr et al., 2011; Hirsch et al., 2014; Donat et al., 2017; Philip et al., 2018; Dirmeyer et al., 2021). Scarce precipitation in preceding season can trigger this feedback loop and amplify hot summer temperature extremes. A few studies have shown that Coupled Model Intercomparison Project Phase 5 (CMIP5) models which represents stronger land–atmosphere coupling in the present climate has most likely tendency to project larger increase in frequencies of future hot extremes (Donat et al., 2018). Moreover, the separation between latent and sensible heat fluxes influences the intensity and duration of extreme heat waves and droughts (Materia et al., 2022; Knist et al., 2017). When soils contain sufficient moisture, evaporation cools the boundary layer by removing heat from the surface. In contrast, dry soils reduce evaporation, causing more energy to convert into sensible heat, which warms the air and intensifies extreme hot events. In conclusion, soil moisture–temperature coupling is critical in transitional evaporative regimes, where soil water scarcity limits evapotranspiration, particularly during summer, creating the ground

https://doi.org/10.5194/egusphere-2026-3206
Preprint. Discussion started: 30 June 2026

for more intense, longer-lasting heatwaves (Koster et al., 2006; Seneviratne et al., 2006; Lorenz et al., 2010; Miralles et al., 2014; Dirmeyer and Halder, 2017).

It is therefore important to understand our state of knowledge about land–atmosphere coupling, given a likely expansion of transitional regimes in the future (Seo and Ha, 2022), while global observational capabilities remain limited and climate models still struggle to accurately represent these processes (Miralles et al., 2019; Quesada et al., 2012).

Observations of soil moisture are primarily obtained through in-situ measurements and microwave remote-sensing satellites. The in-situ stations provide accurate point-scale observations, however, their spatial coverage is extremely limited and uneven (Nguyen et al., 2017; Li et al., 2020; Wu et al., 2021). Satellite retrievals provide broader spatial coverage but are generally limited to the surface layer soil moisture and might have significant uncertainties due to complex land surface conditions, limitations due to the presence of dense cloud cover, and retrieval algorithms (Kim et al., 2018; Mousa and Shu, 2020; Zhuo et al., 2015). To fill these observational gaps, reanalysis products and land surface models have become essential tools for providing continuous spatially gridded global soil moisture data (Li et al., 2020).

Despite the advancements, reliability of reanalysis and model-based soil moisture still remain a main concern in the context of climate change impact studies (Thorne and Vose, 2010). Given its importance in modulating the intensity and duration of hot extremes in many regions of the world (Donat et al., 2017), robust soil moisture datasets are urgently needed to assess environmental impacts and guide adaptation strategies under a changing climate.

Evapotranspiration also remains poorly measured at the global scale because it cannot be directly observed over large spatial domains and must instead be inferred from indirect measurements, remote sensing products, or model simulations, each of which introduces substantial uncertainty (Tran et al., 2023; Yi et al., 2024). Evapotranspiration plays a crucial role in completing the energy/water cycles (Xu et al., 2024). A large amount of incoming solar radiation is used for evapotranspiration in the form of latent heat, regulating the surface energy budget

https://doi.org/10.5194/egusphere-2026-3206
Preprint. Discussion started: 30 June 2026

(Trenberth et al., 2009). The evapotranspiration rate primarily depends on water and energy availability. Potential evapotranspiration (PET) represents the maximum possible water loss to the atmosphere, including water loss from evaporation and plant transpiration—under conditions of unlimited water supply (Thornthwaite, 1948), and depends on temperature, wind, and humidity (Allen et al., 1998). Changes in PET and precipitation modulate the amount of water in the soil. An increase in atmospheric demand for water indicates that PET and evapotranspiration increase. These changes can be very rapid and affect the transition of a water-limited region to an arid-type climate, even if changes in precipitation occur at a slower pace (Cook et al., 2014; Sherwood and Fu, 2014; Xu et al., 2024). Therefore, accurate representation of evapotranspiration and PET is essential for understanding the hydrological cycle and land-atmosphere interaction changes, and for supporting water resource management and drought forecasting. (Dembélé et al., 2020).

With the availability of the vast number of data sources for observations and advancements in data processing methods, further evaluation is essential to guide the effective and efficient use of diverse soil moisture and evapotranspiration datasets. Therefore, the overarching objective of this study is to assess similarities and uncertainties among various observations-based datasets, particularly for variables related to land–atmosphere coupling — namely soil moisture, evapotranspiration, potential evapotranspiration, and 2 m mean air temperature. In addition, this study examines how different datasets represent the individual land and atmospheric coupling pathways, as well as their overall coupling. Here we comprehensively compare various observational data sources, including satellite products (ESA-CCI), satellite-derived estimates (GLEAM versions), reanalysis datasets, and gridded in-situ observations, focusing on Europe.

2 Data and methodology

https://doi.org/10.5194/egusphere-2026-3206
Preprint. Discussion started: 30 June 2026

Data	Data type	Res.	Freq.	Years	Variables
ESA-CCI	Satellite	0.25°	Daily	2003-2022	Surface soil moisture
FLUXCOM	In situ	0.5°	Daily	2003-2020	Latent heat flux, **Evapotranspiration**
E-OBS	Gridded In situ	0.25°	Daily	2003-2022	Surface air temperature, Maximum air temperature, Minimum air temperature, **Potential evapotranspiration**
GLEAM	land evaporation Model	0.25°	Daily	2003-2022	Surface soil moisture, Evapotranspiration, Potential evapotranspiration
SiTHv2	eco-hydrological Model	0.1°	Daily	2003-2020	Surface soil moisture, Evapotranspiration
ERA5/ ERA5-land	Reanalysis	0.25° / 0.1°	Daily	2003-2022	Surface soil moisture, Latent heat flux, Net surface longwave radiation, Net surface shortwave radiation, **Evapotranspiration**, Surface air temperature, Maximum air temperature, Minimum air temperature, **Potential evapotranspiration**
MERRA2	Reanalysis	0.5° × 0.625°	Daily	2003-2022	Surface soil moisture, Evapotranspiration, Surface air temperature, Maximum air temperature, Minimum air temperature, **Potential evapotranspiration**
JRA55	Reanalysis	1.25°	Daily	2003-2022	Surface soil moisture, Evapotranspiration, Surface air temperature, Maximum air temperature, Minimum air temperature, **Potential evapotranspiration**

Table 1: Observations-based datasets used in this study, data type, resolution, temporal frequency, analysis period, and variables. Variables in bold indicate fields that are derived from other provided variables.

https://doi.org/10.5194/egusphere-2026-3206
Preprint. Discussion started: 30 June 2026

2.1 Data

For this observations-based data comparison, all the data are taken for a common period of the recent 20 years (2003-2022, except FLUXCOM and SiTHv2 for which data are only available till 2020) over European IPCC regions (i.e., Northern Europe (NEU), Western central Europe (WCE), Eastern Europe (EEU), and Mediterranean (MED); Fig 1; (Iturbide et al., 2020)). The datasets details are described in the following subsections, and more details regarding the variables, temporal frequency, etc, used in this study are listed in Table 1.

Figure 1: Study area: IPCC reference region (Iturbide et al., 2020)

2.1.1 Global land evaporation Amsterdam Model (GLEAM)

The Global Land Evaporation Amsterdam Model (GLEAM) is a satellite remote sensing-based model designed for the estimation of evaporation and soil moisture globally (Miralles et al., 2011). The version of GLEAM (version 3) used in this study, is available in daily frequency with a spatial resolution of 0.25 ° (Martens et al., 2017). All the components are estimated at each grid using a Priestley and Taylor-based (Priestley and Taylor, 1972) formulation for potential evapotranspiration. GLEAM 3.8a spans a period from 1980 to near-present and is driven by a combination of satellite- and reanalysis-based forcings, whereas GLEAM 3.7b spans from 2003 to the present and is driven entirely by satellite-based forcing data.

2.1.2 ECMWF reanalysis v5 (ERA5)

ERA5 is the fifth generation of the ECMWF reanalysis based on the Integrated Forecasting System (IFS) version CY41R2. Measurements from various observations systems are assimi-

https://doi.org/10.5194/egusphere-2026-3206
Preprint. Discussion started: 30 June 2026

lated into the atmospheric model using a 4D-Var scheme (Hersbach et al., 2020). ERA5 provides 137 hybrid sigma/pressure levels of the atmosphere from the surface up to 1 Pa. The grid resolution is 31 km. Data are provided at a hourly frequency and provide global spatial coverage from 1940 until the present.

ERA5-Land is produced by rerunning the land component from ERA5 atmospheric reanalysis with a higher spatial resolution of 0.1 °. The model used for ERA5-Land is the tiled ECMWF Scheme for Surface Exchanges over Land incorporating land surface hydrology (H-TESSEL) (Muñoz-Sabater et al., 2021), forced by the ERA5's atmospheric fields. Data are provided from 1950 to the present at an hourly frequency over land regions only.

2.1.3 European Space Agency Climate Change Initiative (ESA CCI) soil moisture

The ESA CCI soil moisture dataset is provided by the Climate Change Initiative program of the European Space Agency. ESA CCI, as a satellite product, only provides the surface layer soil moisture and is primarily composed of three types of daily frequency dataset sources, i.e., active, passive, and active-passive combined microwave products (Dorigo et al., 2017; Gruber et al., 2019; Preimesberger et al., 2020). Here, we select the daily combined microwave products of version 8.1 with a spatial resolution of 0.25 °. The data is available from 1991 until recent time.

2.1.4 E-OBS

The E-OBS dataset (Cornes et al., 2018) provides daily gridded surface variables at 0.1° and 0.25° resolution over Europe covering the area 25°N–71.5°N, 25°W–45°E. The dataset is prepared by collection from station data collated by the ECA&D (European Climate Assessment & Dataset) initiative (Klein et al., 2002). In the present study, we use the dataset's version 29 at 0.25° resolution for mean, maximum, and minimum temperatures at 2 meters.

https://doi.org/10.5194/egusphere-2026-3206
Preprint. Discussion started: 30 June 2026

2.1.5 FLUXCOM

FLUXCOM uses machine learning to merge energy flux measurements from FLUXNET eddy covariance towers with remote sensing and meteorological data to estimate global gridded net radiation, latent heat flux, sensible heat flux, and their uncertainties (Jung et al., 2019). The FLUXCOM provides data in two resolutions: high resolution of 0.0833° using MODIS remote sensing data, and low resolution of 0.5° using remote sensing and meteorological data. It uses seasonal vegetation variables and indices from either measured at the flux tower sites or retrieved from the ERA-Interim (Dee et al., 2011). In this study, we use a 0.5° resolution latent heat flux to calculate evapotranspiration.

2.1.6 Simple Terrestrial Hydrosphere model, version 2 (SiTHv2)

The Terrestrial Hydrosphere model, version 2 (SiTHv2) is an eco-hydrological model. It is driven by multi-source satellite observations and hydrometeorological variables from reanalysis data. It provides daily global evapotranspiration and soil moisture at a 0.1° spatial resolution (Zhang et al., 2024). The global soil type used in this model is acquired from the Harmonized World Soil Database version 1.2 (Wieder et al., 2014). For vegatation dynamics, the leaf area index from the European Geoland2/BioPar project Version 2 is used (Baret et al., 2013). Annual land cover dynamics are taken from the Historic Land Dynamics Assessment+ product (Winkler et al., 2021). The Global Land Surface Satellite product (Liang et al., 2021) is used for surface albedo and emissivity observations. Daily air temperature and air pressure data are taken from the Multi-Source Weather product (Beck et al., 2022), and radiation and precipitation data from ERA5 (Muñoz-Sabater et al., 2021).

2.1.7 Japanese 55-year reanalysis (JRA-55)

The Japan Meteorological Agency (JRA55) reanalysis JRA-55 provides land analyses by running an offline land model with forcing from an atmospheric model (Kobayashi et al., 2015). The data are available in a 320 × 640 Gaussian grid from 1958 to 2024. We have taken surface soil moisture, evapotranspiration, surface air temperature, maximum air temperature, and minimum air temperature from JRA55 in this study.

https://doi.org/10.5194/egusphere-2026-3206
Preprint. Discussion started: 30 June 2026

2.1.8 Modern-Era Retrospective analysis for Research and Applications version 2 (MERRA2)

Modern-Era Retrospective analysis for Research and Applications version 2 (MERRA2) is a global atmospheric reanalysis produced by NASA's Global modeling and Assimilation office (Gelaro et al., 2017). It has 0.5° (latitude) × 0.625° (longitude) spatial resolution, with vertical 72 hybrid sigma-pressure layers from the surface to 0.01 hPa at hourly frequency. We have used surface soil moisture, evapotranspiration, surface air temperature, maximum air temperature, and minimum air temperature in this study.

2.2 Methodology

To study the coupling metrics of land and atmosphere in better possible way, the ERA5-land and SiThv2 data variables are re-gridded to the resolution of the ERA5 data. Similarly, the ESA-CCI and E-OBS data are re-gridded to the FLUXCOM resolution. In the JRA55 surface soil moisture data, the first day of each month shows abnormally low values. This bias is shown in Figure 2, but these values are excluded and converted to Nan values in all the successive analyses. Similarly, in both the Gleam versions (i.e., 3.7 b and 3.8a), the evapotranspiration and potential evapotranspiration show abnormally low values for June 6 and June 7 each year in some regions (Figure 2), and are also converted to Nan values. The surface soil moisture from ESA-CCI is only taken from May to November: in fact, a large fraction of missing data is present over most European regions from December to April, mainly due to frozen soils and snow cover, which greatly limit the accuracy of the microwave measurements (Zheng et al., 2023; Preimesberger et al., 2020, 2025) (figures not shown).

For the datasets lacking evapotranspiration and potential evapotranspiration, these variables have been calculated as in Allen et al.,1998:

$$Evapotranspiration = \frac{LHF}{2.501 - (2.361 \times 10^{-3}) \times T} \quad (1)$$

This equation takes the density of water equal to 1000 $kg \cdot m^{-3}$. Latent heat flux (LHF) and corresponding temperature (T) from observations or reanalysis are in units of $MJ \cdot m^{-2} s^{-1}$

https://doi.org/10.5194/egusphere-2026-3206
Preprint. Discussion started: 30 June 2026

and °C, respectively, which gives evapotranspiration in units of $kg \cdot m^{-2}s^{-1}$. It is converted to mm/day by multiplying the value by 86400.

PET (Except for GLEAM data, in which PET is provided as a variable to download directly from the data source) is calculated using daily air temperature, maximum temperature, and minimum temperature using the Hargreaves equation (Hargreaves and Samani, 1982), Baier's equation (Baier and Robertson, 1965), and Thornthwaite´s equation (Thornthwaite, 1948) based on the Python package xclim (Logan et al., 2022). Penman-Monteith (Allen et al., 1998) equation based on the Python package PyETo., that uses several atmospheric parameters, is used as well (Note that only the Hargreaves method is shown in the main figures and the others are included in supplementary figures for PET analysis only).

Equations for each method are as follows:

PET by (Hargreaves and Samani, 1982):

$$\begin{aligned} PET &= K \times SR \times (T + 17.8) \\ &= K \times K_{SR} \times R_a \times (T + 17.8) \times \sqrt{Tmax - Tmin} \end{aligned} \tag{2}$$

Where K is a constant, SR is solar radiation, and T is the daily air temperature in °C units. K_{SR} is a constant, R_a is extraterrestrial radiation, and Tmax and Tmin are the daily maximum and minimum air temperature, respectively.

PET by (Baier and Robertson, 1965):

$$PET = 0.094 \times (-87.03 + 0.928 \times Tmax + 0.933 \times (Tmax - Tmin) + 0.0486 \times R_a \tag{3}$$

PET by (Thornthwaite, 1948): The xclim Python package calculates PET directly from Tmax and Tmin through a series of steps. First, it determines the annual Heat Index (I) using the following formula:

$$I = \sum_{i=1}^{12} \left(\frac{T}{5}\right)^{1.514} \tag{4}$$

https://doi.org/10.5194/egusphere-2026-3206
Preprint. Discussion started: 30 June 2026

In the xclim Thornthwaite method, PET is estimated monthly, assuming a 30-day month with 12 theoretical sunshine hours per day. These values are then adjusted based on the actual month length and theoretical sunshine hours for the specific latitude, using the following equation:

$$PET = 16 \times \left(\frac{10 \times T}{I}\right)^{\alpha} \times \left(\frac{N}{12} \times d\right) \tag{5}$$

where N is the theoretical sunshine hours for each month, and d is the number of days for each month. α is calculated as:

$$\alpha = 675 \times 10^{-9} \times I^3 - 771 \times 10^{-7} \times I^2 + 1792 \times 10^{-5} \times I + 0.49239 \tag{6}$$

PET by Penmann-Monteith method:

$$PET = \frac{0.480 \times \Delta \times (R_n - G) + \gamma \times \frac{900}{T+273} \times U_2 \times (e_s - e_a)}{\Delta + \gamma \times (1 + 0.34 \times U_2)} \tag{7}$$

where R_n is net surface radiation in units of $MJ \cdot m^{-2}s^{-1}$, G is the soil heat flux in $MJm^{-2}s^{-1}$, T is 2 meter air temperature in $^{\circ}C$, U_2 is the wind speed at 2 meter height in m/s, e_s and e_a are saturation vapor pressure and actual vapor pressure respectively in kPa, Δ is the slope of the saturation vapor pressure curve in $kPa/^{\circ}C$, and γ is the psychometric constant in $kPa/^{\circ}C$.

3 Results

3.1 Annual cycle and interannual variation over European regions

To understand the seasonal variation throughout the year, we first analyze the annual cycle at the daily scale for surface soil moisture (SSM), evapotranspiration (EVT), and potential evapotranspiration (PET) across the four IPCC-defined regions: NEU, WCE, EEU, and MED (Iturbide et al.,2020; Fig. 2). JRA55 indicates abnormally low values of SSM on each month's first day, which might be due to model initialization (no such documentation of this error is found in the literature). This issue still might affect their monthly average SSM data, and therefore, the users should be aware of it before using the data in their analysis.

https://doi.org/10.5194/egusphere-2026-3206
Preprint. Discussion started: 30 June 2026

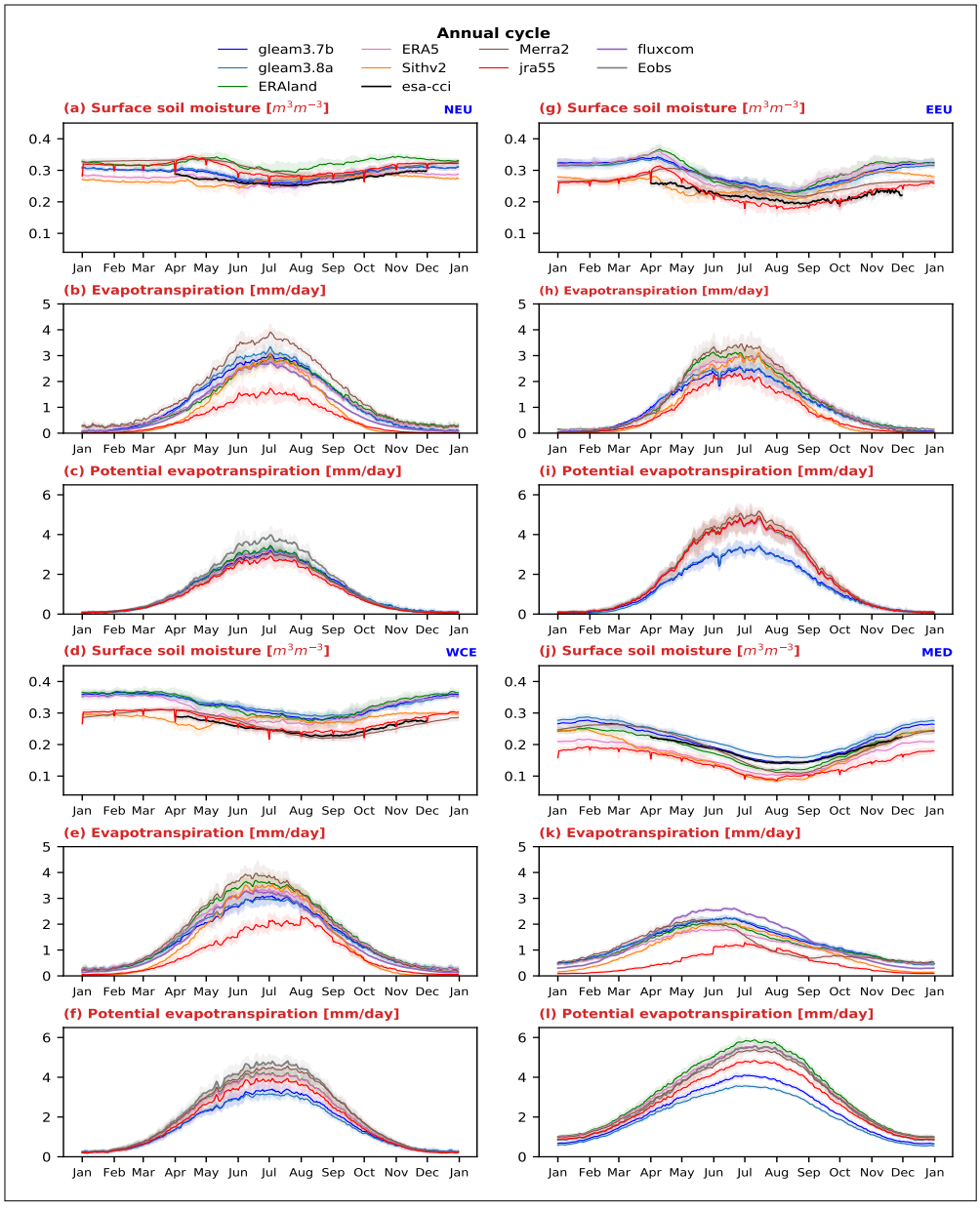

Figure 2: Daily annual cycle of SSM (surface soil moisture), EVT (evapotranspiration), and PET (potential evapotranspiration) over four IPCC European regions (NEU: **(a)**, **(b)**, **(c)**; WCE: **(d)**, **(e)**, **(f)**; EEU: **(g)**, **(h)**, **(i)**; MED: **(j)**, **(k)**, **(l)**). The 25th–75th percentile ranges are shown as shaded regions for each data point.

https://doi.org/10.5194/egusphere-2026-3206
Preprint. Discussion started: 30 June 2026

The four regions indicate similar annual cycle for all datasets for each variable, with summer characterized by drier soil moisture, elevated evapotranspiration, and higher PET.

NEU SSM (Fig. 2a) shows low seasonal variability, with drier decreases during winter and then increases to reach a spring peak, following snow melt. Then summer gets drier, and a secondary wet phase takes place in autumn. As this region experiences wet summers, the seasonal variation of SSM is low, even though the EVT (Fig. 2b) and PET (Fig. 2c) annual cycle indicate a gradual increase during spring and summer. The factual lack of summer water stress also explains the minimal difference between PET and EVT over this region, suggesting that NEU lies in an energy-limited evaporative regime. For SSM annual cycle (Fig. 2a), SiTHv2 and MERRA2 have very different annual variation than rest of the data and it is same for all regions. For EVT (Fig. 2b), there is a big difference between MERRA2 and JRA55 (by the factor of 2 mm/day) during summer, while other datasets are much closer to each other and this is also seen for EEU and WCE. For PET (Fig. 2c), E-OBS represents the highest peak and JRA55 the lowest during summer while other datasets are very similar to each other.

Similarly, for EEU, the SSM annual cycle (Fig. 2g) begins with almost stable values in entire winter, following a steady increase in SSM that peaks in early spring. This is succeeded by a sharp decline at the start of summer, with continued drying through late summer, before SSM rises again to reach a secondary peak in late autumn. The lowest EVT (Fig. 2h) occurs during winter, increasing through spring and peaking in summer, followed by a gradual decline during autumn. Over EEU, GLEAM 3.7b and 3.8a show abnormally low EVT and PET values (Fig. 2i) on June 6th and 7th of each year, therefore, these dates are removed from the GLEAM datasets in the following analysis. The PET annual cycle variation during summer for both GLEAM versions about 2 factors less than rest of the datasets which coincide with each other. PET variation follows similar pattern as EVT in both the GLEAM datasets, while summer EVT is considerably lower than summer PET in the other datasets.

SSM variability (Fig. 2d) in the WCE region shows a similar winter no variability as EEU (Fig. 2g), followed by a gradual decline from spring through summer and mid-autumn, and a

https://doi.org/10.5194/egusphere-2026-3206
Preprint. Discussion started: 30 June 2026

renewed increase toward late autumn and early winter. In contrast, EVT (Fig. 2e) and PET (Fig. 2f) are characterized by low values in winter, a steady increase through spring, and a pronounced peak during summer, after which both variables decrease progressively into autumn. This seasonal evolution reflects a coherent annual pattern, with soil moisture variability being highest during the cooler seasons, while evapotranspiration and potential evapotranspiration are at their maximum during the warmest months of the year. During summer, all the datasets shows very distinct peak for PET while all of them are calculated using same equation (except GLEAM versions) and it is also seen in the case for MED.

The driest soil is found in the MED region (Fig. 2j), especially in the summer, while PET (Fig. 2l) is the highest among all regions. During the summer, there is often not enough soil water available to meet the atmospheric demand, making MED a water-limited region. Therefore, the EVT values are lower during summer compared to other regions despite the higher solar radiation and temperatures. The soil moisture values are similar across datasets, except for JRA55, that shows lower values, and Sithv2, characterized by a more pronounced seasonal cycle. EVT is also comparable among datasets, apart from an early dip in MERRA in mid-summer and a delayed summer peak accompanied by very low values for JRA55. PET follows the temperature annual cycle, with large variability across datasets during the summer.

In Supplementary Fig. A1, we compare the different PET calculations (only for ERA5land) for all the regions. Baier's method shows a notably narrower range, with PET values remaining at zero during winter and autumn, before abruptly peaking in summer to align with Hargreaves-derived PET values. The Penman-Monteith method applied to ERA5 and ERA5-Land data shows a slight shift in the timing of the peak relative to the other PET estimates. Hargreaves-based PET also closely matches the GLEAM (3.7b and 3.8a) PET estimates for NEU. Baier's method in MED does not exhibit extended zero values in spring or autumn but instead follows a pattern similar to that of the Hargreaves and Penman-Monteith methods.

There exist substantial differences in the seasonal patterns of PET derived from various estimation methods. These discrepancies are largely attributed to the complexity of the underlying

https://doi.org/10.5194/egusphere-2026-3206
Preprint. Discussion started: 30 June 2026

equations and the input variables involved. Generally, the more complex the method, the greater the potential for biases introduced by uncertainties in the input variables. For example, while the Penman-Monteith method is considered physically comprehensive, accounting for temperature, humidity, radiation, and wind speed, it is also more susceptible to compounded errors due to biases in these multiple inputs. Such issues have been well-documented in previous studies (Li et al., 2022; Trajkovic, 2007; Moratiel et al., 2020).

In contrast, the Hargreaves method offers a simpler and more robust alternative, relying solely on temperature for PET estimation. Given its simplicity and reduced vulnerability to multi-variable bias, we selected the Hargreaves method for PET representation in the following analysis. This choice provides a relatively simple but robust method for intercomparison and interpretation across datasets and regions, without the added uncertainty introduced by more complex formulations. Additionally, applying the Hargreaves method across all datasets is necessary for consistency in this study, as it ensures a uniform approach to PET estimation, which would be more complicated with the Penman-Monteith method due to larger uncertainties across different data sources.

To gain an extensive understanding of the climate dynamics, it is crucial to examine the interannual variability of each variable and the relationships between them, especially in the context of recent trends. This analysis focuses specifically on the summer months—June, July, and August (Fig. 3, Fig. 4).

Generally, SSM cross-correlation is consistently high across all regions and datasets, indicating strong agreement. Likewise, PET shows good association across datasets, probably due to the low uncertainty in temperatures, but less so for the Mediterranean. EVT is the variable that shows the lowest agreement among datasets for all regions .

Over NEU, across all the datasets SSM varies (Fig. 3a) from around 0.22 m^3m^{-3} to 0.35 m^3m^{-3} exhibiting strong interannual variability. All the datasets show the the wettest summers during 2012 and 2017, while the driest occurred in 2006 and 2018. The strong drought event is

https://doi.org/10.5194/egusphere-2026-3206
Preprint. Discussion started: 30 June 2026

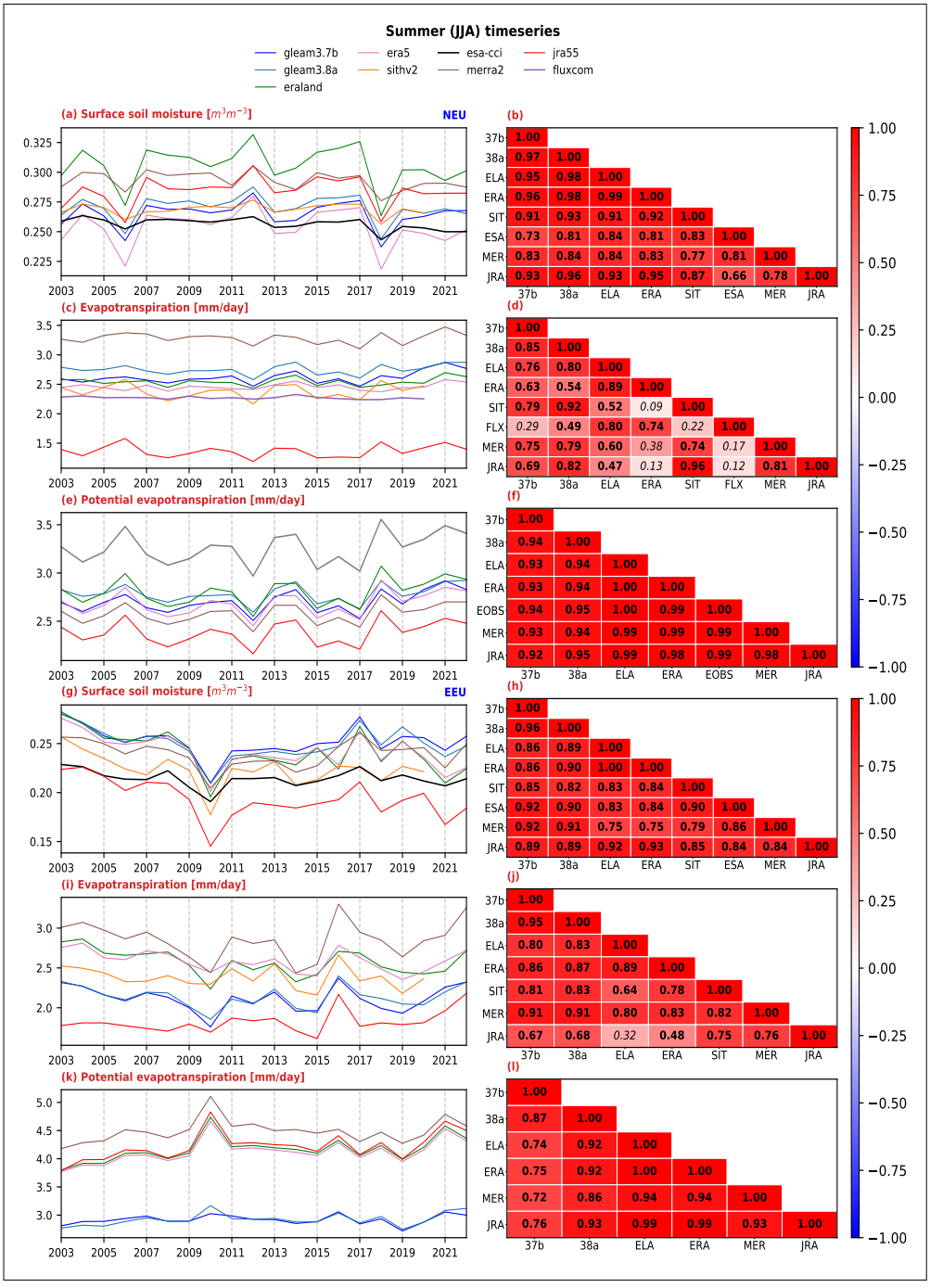

Figure 3: Interannual variation (in left) and Correlation composite matrix (right) of ssm, evt, and pet over NEU ((**a**), (**b**), (**c**), (**d**), (**e**), (**f**)), EEU ((**g**), (**h**), (**i**), (**j**), (**k**), (**l**)). The correlation coefficient values in bold are significant at 95% level and rest are in *italic*.

https://doi.org/10.5194/egusphere-2026-3206
Preprint. Discussion started: 30 June 2026

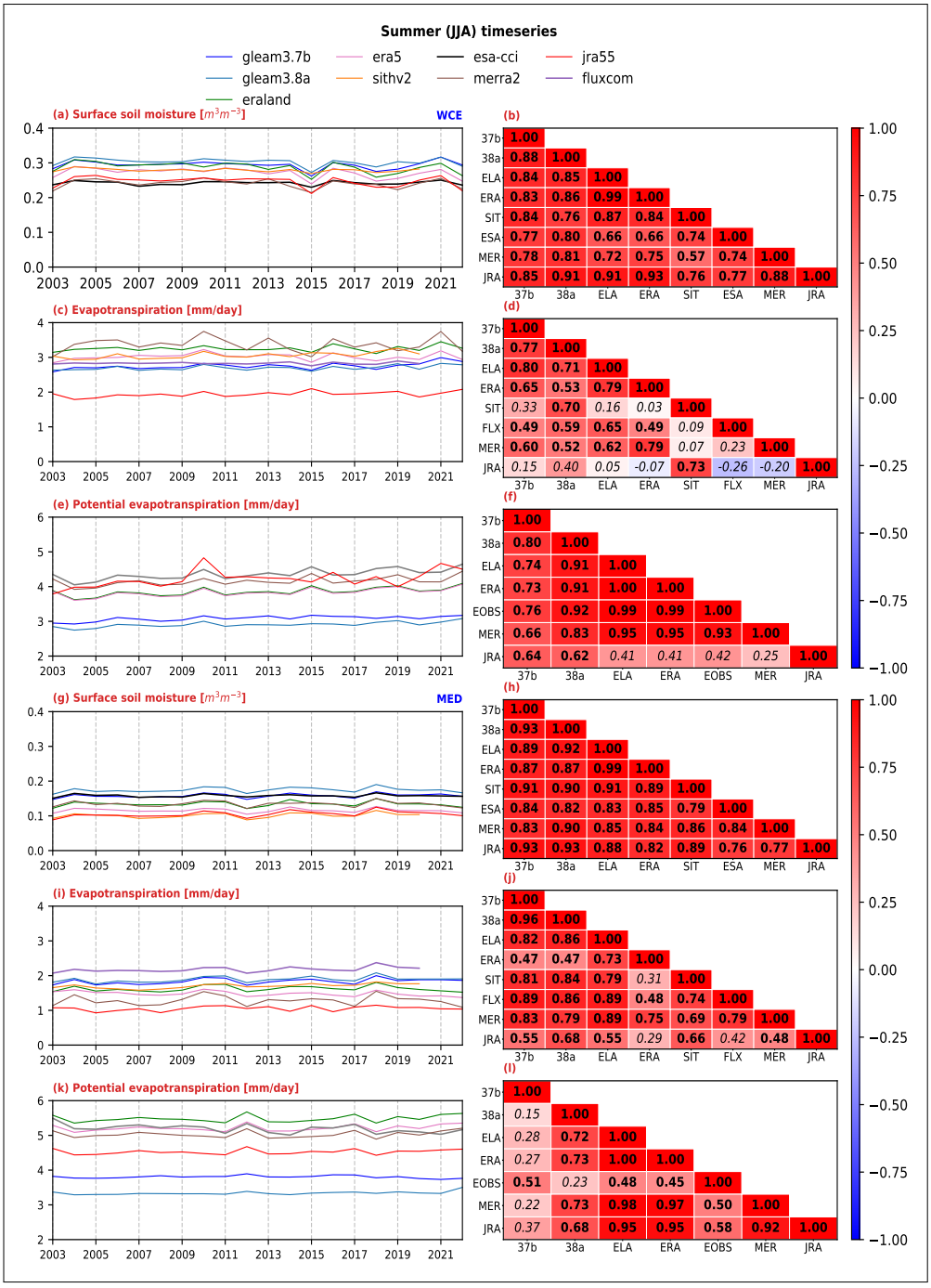

Figure 4: Same as Fig. 3, but for WCE ((**a**), (**b**), (**c**), (**d**), (**e**), (**f**)), MED ((**g**), (**h**), (**i**), (**j**), (**k**)).

https://doi.org/10.5194/egusphere-2026-3206
Preprint. Discussion started: 30 June 2026

mentioned in many previous studies (Rousi et al., 2023; Bakke et al., 2020). EVT interannual variability (Fig. 3c) is less pronounced compared to SSM. However, when the SSM is drier, the EVT is higher, and vice versa, as expected in energy-limited regimes. Similarly, PET (Fig. 3e) indicated high interannual variability among all the datasets, with atmospheric water demand that was the highest for the dry summers of 2006 and 2018, and also 2021 which was still hot but wetter than the previous ones, allowing higher evapotranspiration (Fig. 3e). The correlation matrices for SSM and PET indicate highly positive correlation values among all the datasets, while weaker correlation are shown for EVT in case of SiTHv2, MERRA2, JRA55 with ERA5, FLUXCOM with GLEAM 3.7b, SiTHv2, MERRA2, and JRA55 (Fig. 3d).

Over EEU, the interannual variability is higher for SSM (Fig. 3g) and EVT (Fig. 3i) compared to PET (Fig. 3k). All the datasets show driest SSM during 2006, 2010, 2018, and 2021, and wettest during 2003, 2008, 2017, 2019, and 2022 (except in JRA55, where few of these are shifted by a year). The high EVT are seen during 2004, 2007, 2011, 2013, 2016, 2022 and low in 2003, 2006, 2010,2012, 2014, 2015, 2017, 2019. All the datasets well captures the well known extremely hot and dry summer of 2010 over EEU, that was subject of many previous studies (Barriopedro et al., 2011; Lhotka and Kyselỳ, 2015; Lebedeva et al., 2016). During the summer of 2010, the soil is so dry that there is no moisture left to meet the enormous atmospheric demand of water supply associated with the severe heat hitting the region. For this region, all the datasets are highly positively correlated among each other for all the variables except JRA55 with ERA5land for EVT.

WCE and MED show relatively smaller interannual variability for all the variables. In both regions, SSM (Fig. 4a,g) dips in the summer of 2003 and 2022, known to be characterized by widespread hot and dry conditions (Dosio et al., 2023; Herrera-Lormendez et al., 2023; Rebetez et al., 2006), while summer 2004 and 2021 (only for WCE) were wet (Fig. 4a,g) and relatively cool (Fig. 4e,k) in both regions. In WCE, the extremely hot and dry summer 2015 (Orth et al., 2016; Hoy et al., 2017) is also detected by all the soil moisture datasets. Conversely, responses are different in terms of the EVT, as shown by the timeseries (Fig. 4c). For example, JRA55 and SiTHv2 show increasing evaporation during low SSM years, while MERRA2 show peaks

https://doi.org/10.5194/egusphere-2026-3206
Preprint. Discussion started: 30 June 2026

in EVT not detected by any other dataset. For EVT, the datasets SiTHv2, FLUXCOM, JRA55 and MERRA2 are weakly correlated with other datasets and among themselves too. PET for WCE (Fig. 4e) interannual variability follows similar pattern for all datasets except JRA55 which reflects in the correlation matrix (Fig. 4f).

MED region shows low interannual variability and the lowest SSM (Fig. 4g) and EVT (Fig. 4i) ranges, while PET (Fig. 4k) is the highest indicating the largest atmospheric evaporative demand among the four regions. Apart from the already mentioned 2003 and 2022, summers 2012 and 2017 are characterized by low soil moisture and evapotranspiration, following anomalously warm and dry conditions (Wilcox et al., 2018; Kew et al., 2019). Wetter summers like 2004, 2014, and 2018 (Ratna et al., 2017; Beillouin et al., 2020) see a peak in SSM and EVT, and a trough in PET. Similar to all the other regions the SSM (Fig. 4h) data indicate very high corelation among themselves. The correlation matrix (Fig. 4j) shows ERA5 and JRA55 weakly correlated with most of the data which is similarly found over all the regions except EEU. The correlation matrix of PET in MED (Fig. 4l) shows GLEAM 3.7b is weakly correlated with all the data except E-OBS, and E-OBS is poorly correlated with GLEAM 3.8a.

The comparison of the different PET methods for interannual variation (Fig. A2) reveals a wide range of PET variability, with some methods exhibiting inconsistent interannual patterns for the same region and even within the same dataset. Across all regions, PET derived from the Thornthwaite method consistently exhibits the highest values (except for MED). Only for MED, Penman–Monteith method indicates different pattern than rest of the methods and GLEAM versions. GLEAM (both versions) systematically produces lower PET values across regions (except for NEU).

The correlation matrices (Fig. A3) show strong agreement among datasets for all the regions except for MED, suggesting that interannual PET variability in these regions is relatively insensitive to methodological differences. For MED, the Penman–Monteith method shows negative correlation coefficient with GLEAM both versions, Hargreaves and Baier's methods, while PET from the rest of the methods indicate high positive correlation with GLEAM 3.8a and

https://doi.org/10.5194/egusphere-2026-3206
Preprint. Discussion started: 30 June 2026

among themselves.

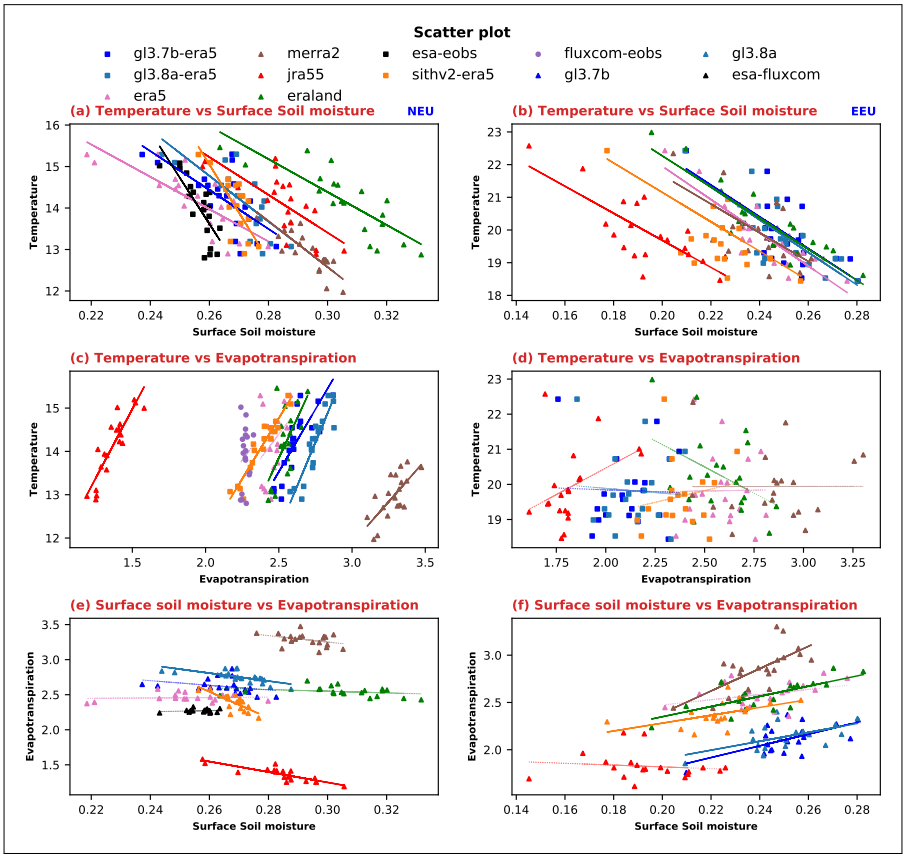

Figure 5: Scatter plot and linear regression(on the left for NEU and on the right for EEU) between SSM, EVT, TAS. The thick line indicates linear regression significance at 95% level, and the dashed line indicates the regression is not significant.

3.2 Land-atmosphere coupling

We now explore the relationships among these variables to gain deeper insights into the spatial variability patterns of land–atmosphere coupling. Here, we first investigate the scatter plots and linear regression analysis (Fig. 5 and Fig. 6) between 2m mean air temperature (TAS), SSM, EVT. Here, as GLEAM 3.7b, GLEAM 3.8a, and SiTHv2 do not have TAS data, TAS from ERA5 is used to study the land-atmosphere coupling. Similarly, as FLUXCOM, E-OBS, and ESA-CCI are based on the in situ data, the couplings are shown for dataset combinations

https://doi.org/10.5194/egusphere-2026-3206
Preprint. Discussion started: 30 June 2026

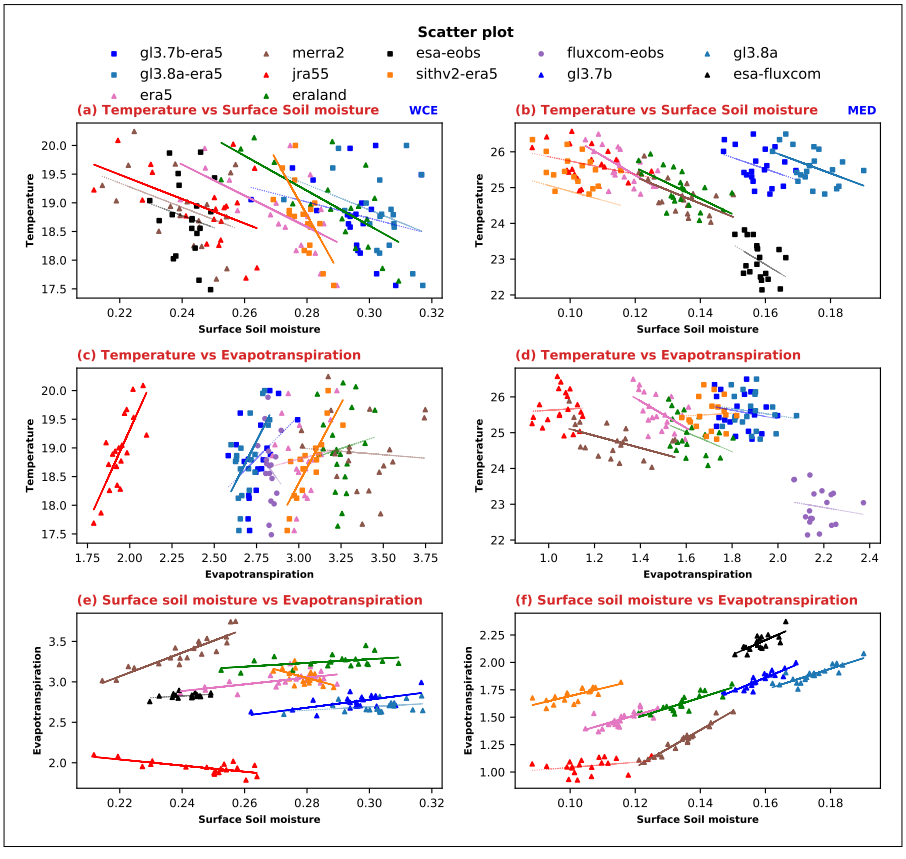

Figure 6: Same as Fig. 5, but for WCE (left), MED (right).

https://doi.org/10.5194/egusphere-2026-3206
Preprint. Discussion started: 30 June 2026

representing gridded observations. For this analysis, these three datasets are shown for the period 2003-2020.

Previous studies have identified transitional evaporative regimes as hot spots of soil moisture–temperature coupling (Gevaert et al., 2018; Schwitalla et al., 2025). In these regions, evaporation is both sufficiently variable and strongly controlled by soil moisture availability, allowing it to significantly influence atmospheric variability. In contrast, soil moisture is generally not a limiting factor in wetter regions, where evaporation is predominantly driven by radiation. Meanwhile, in drier regions, both soil moisture and evaporation exhibit limited variability, reducing their influence on air temperature dynamics. The SSM and EVT relation represents the terrestrial leg of the coupling. In contrast, EVT and TAS relations explain the atmosphere leg of the coupling, and SSM and TAS relations indicate the combination of both,i.e., land-atmosphere coupling (overall coupling).

In general, during summer, evaporation increases with increasing temperature, and this leads to a reduction in the surface soil moisture. When soil water starts being scarce, plants reduce transpiration. Therefore, despite high radiation and temperature, evapotranspiration decreases and soil moisture too. This, in turn, increases the gap between EVT and PET (the latter is not limited by water) actually becomes substantial. This will in turn lead the boundary layer to warm further due to scarce evaporative cooling making that particular region prone to longer-lasting and more intense heatwaves (Mueller and Seneviratne, 2012; Materia et al., 2022). This feedback mechanism can be durable and lead to further increases in temperature and finally drought conditions (Miralles et al., 2019).

Over NEU, SSM decreases with increasing TAS during summer across all datasets (Fig. 5a). However, the atmospheric coupling indicates a positive relation (Fig. 5c), suggesting that EVT is primarily controlled by available energy rather than SSM. The weak dependence of EVT on SSM (Fig. 5e) further supports the characterization of NEU as an energy-limited region during summer, where enhanced solar radiation drives evaporation even under decreasing soil moisture conditions.

https://doi.org/10.5194/egusphere-2026-3206
Preprint. Discussion started: 30 June 2026

For EEU, the coupling between TAS and SSM, as well as the land coupling, shows significant relationships across most datasets (Fig. 5b,f), while the atmospheric coupling remains largely insignificant (Fig. 5d). This indicates that although SSM and TAS are coupled, variations in SSM do not consistently translate into changes in EVT. The lack of a coherent TAS–EVT relationship likely reflects strong spatial heterogeneity among datasets, and the area average of this nullifies both positive and negative relations.

Over WCE, correlations are generally significant across all coupling components. The atmospheric coupling (Fig. 6c) exhibits a steep positive slope, indicating that relatively small changes in EVT are associated with comparatively large TAS responses (except MERRA-2 and FLUXCOM) which reflects in the overall coupling (Fig. 6a) with steep negative slopes indicating small changes in SSM lead to a big change in TAS. At the same time, the land coupling (Fig. 6e) shows a decrease in EVT with declining SSM (except SiTHv2 and JRA55 which show negative slopes), identifying WCE as a predominantly water-limited region during summer.

In the MED region, the negative atmospheric coupling (Fig. 6d) indicates a water-limited regime, where EVT is decreasing despite of increasing TAS. The overall and terrestrial coupling (Fig. 6b,f) show patterns similar to WCE but with steeper slopes, pointing to a stronger moisture limitation. Although correlations across coupling components are generally significant, land–atmosphere interactions in MED are primarily governed by SSM availability rather than energy, resulting in suppressed EVT during summer and enhanced near-surface warming.

Using scatter plot and linear regression analysis, we examined the general picture of land and atmosphere coupling during summer in the four European IPCC regions. Although the datasets varied in their ranges, they exhibited mostly similar coupling relationship within each region. However, a limitation of this analysis is that it may mask important spatial variations within regions, as strong localized relationships can dominate and skew the area-averaged results, as observed in EEU for the relationship between TAS and EVT. Therefore, a more detailed spatial analysis of land–atmosphere coupling is necessary to capture regional heterogeneity

https://doi.org/10.5194/egusphere-2026-3206
Preprint. Discussion started: 30 June 2026

and underlying patterns better, and here we investigated the correlation (Fig. 7) and regression (Fig. 8) among TAS, EVT and SSM over the entire Europe.

The spatial coupling analysis also indicates that, irrespective of actual values of the variables, all the datasets represent similar relationships among the variables, except JRA55, where the land coupling and the atmospheric coupling pattern do not match the rest of the datasets. Overall, the spatial coupling relations over Europe match the regional spatial averaged analysis that we discussed earlier, with Northern Europe being an energy-limited region and the southern part being a water-limited region. For example, if we focus on a water-limited region like Spain, then the atmospheric coupling represents a significant negative relation, indicating that as the temperature rises during summer, the evaporation actually decreases. The land coupling represents that the increase in soil moisture leads to an increase in evapotranspiration. Similarly, over an energy-limited region like Scandinavia, where the pattern is being reversed as compared to Spain. Therefore, when we investigate the overall coupling of temperature with soil moisture, it is negative all over Europe, but in northern Europe, the energy is limited, therefore, the increase in temperature is leading to enhanced atmospheric demand of water, which is then met by the water supply via evapotranspiration from soil moisture. In contrast, for southern Europe, the soil moisture is the limiting factor during summer, when the temperature is high, but still the low soil moisture can not meet the atmospheric demand for water, which further keeps rising the temperature. Here, we found that the southern part of France has a significant positive relation between SSM and EVT (land coupling), as well as between EVT and TAS (atmospheric coupling).

4 Discussion and Conclusions

In this study, we examine the similarities and differences among multiple gridded observations-based datasets in capturing the interannual variability of key surface parameters involved in land-atmosphere coupling, such as the surface soil moisture, evapotranspiration, potential evapotranspiration, and 2m air temperature, across Europe during summer. We further performed an extensive analysis of differences and similarities in the representation of coupling relationships

https://doi.org/10.5194/egusphere-2026-3206
Preprint. Discussion started: 30 June 2026

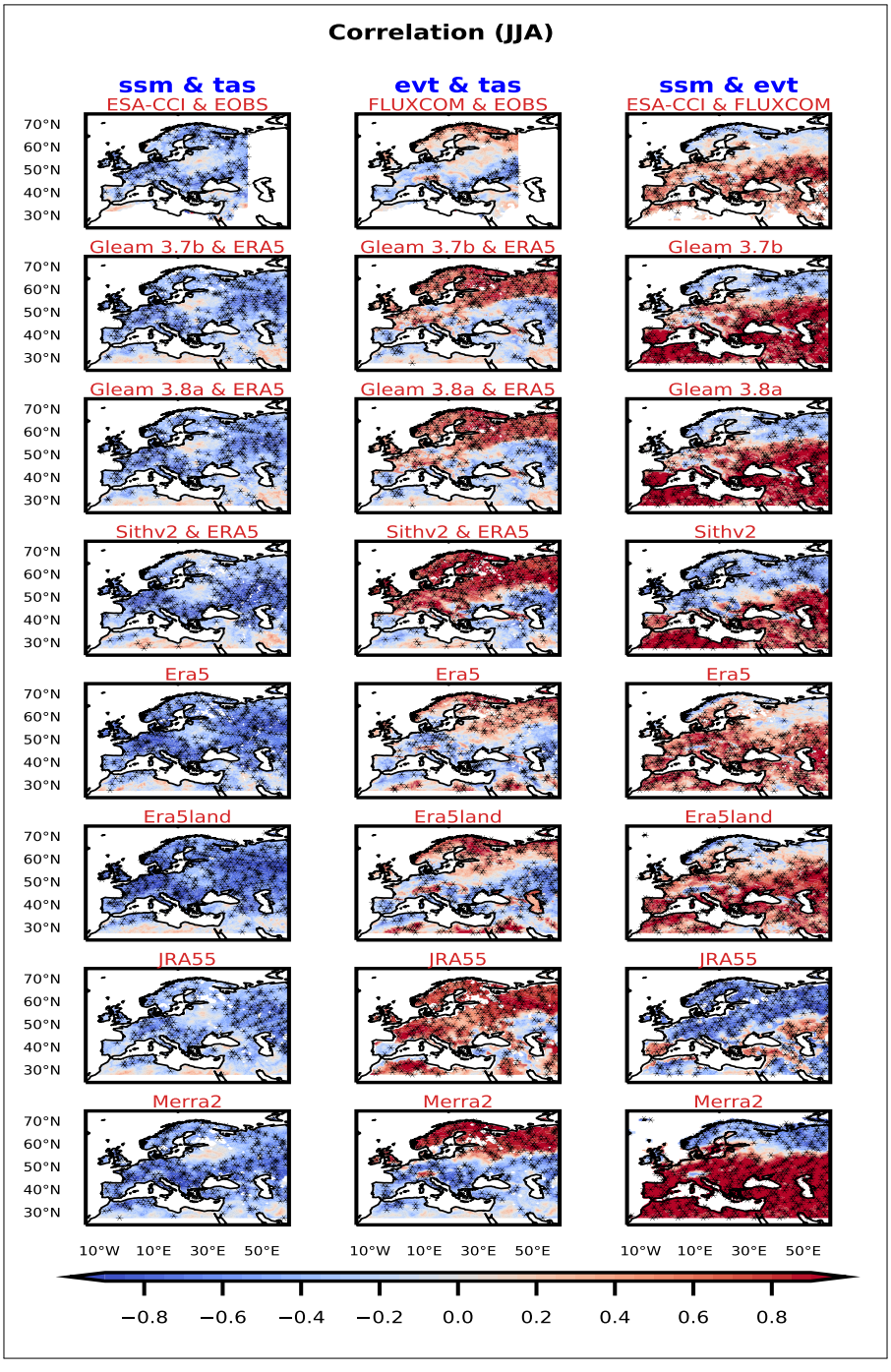

Figure 7: Correlation map of: **(left)** SSM and TAS, **(centre)** EVT and TAS, and **(right)** SSM and EVT. The black dots represent correlation coefficients significant at 95% level.

https://doi.org/10.5194/egusphere-2026-3206
Preprint. Discussion started: 30 June 2026

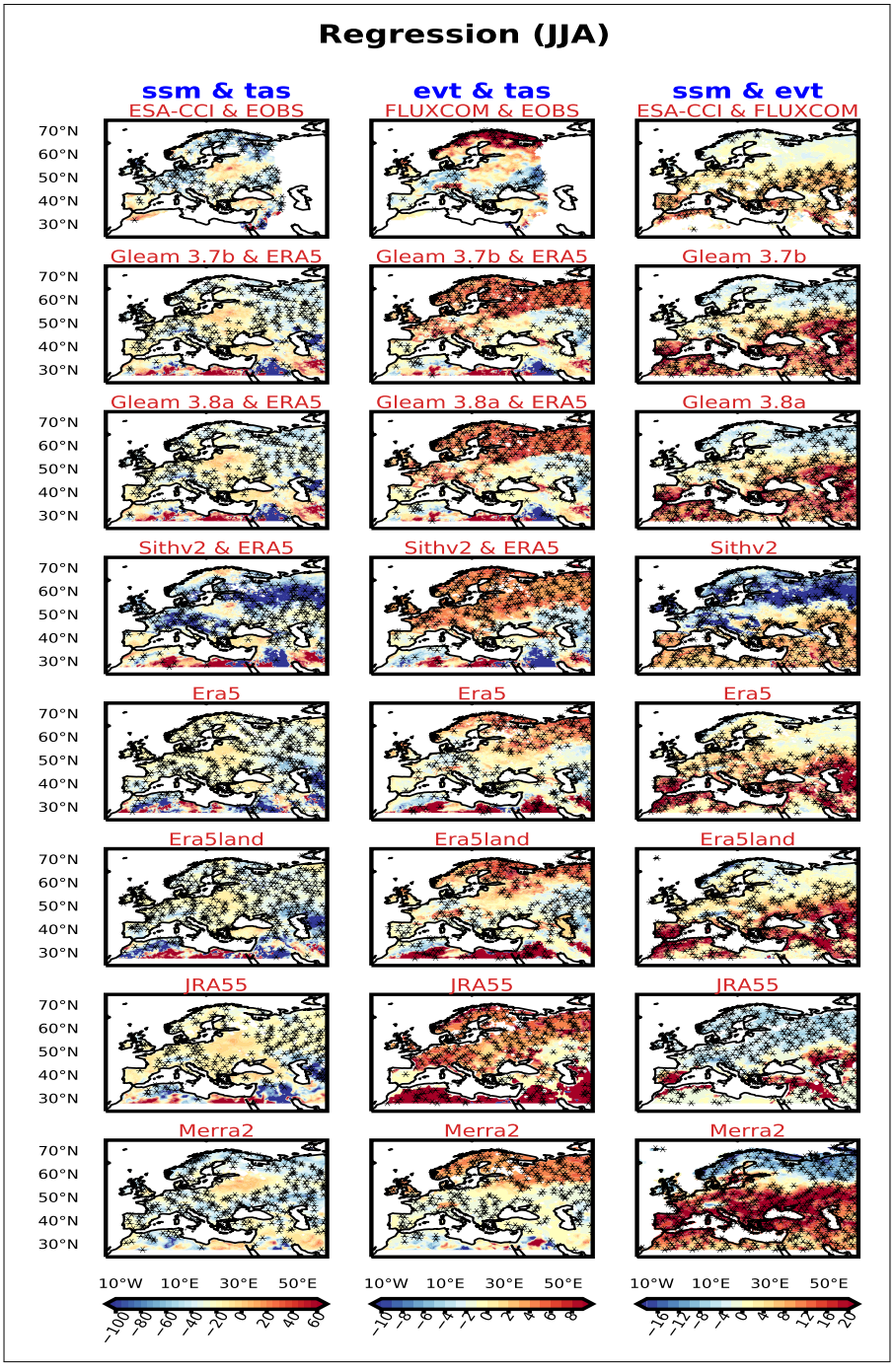

Figure 8: Same as Fig. 7, but showing the slope of the linear regression.

https://doi.org/10.5194/egusphere-2026-3206
Preprint. Discussion started: 30 June 2026

at the land-atmosphere interface, whose impact on heat extremes is well established for regions in transitional evaporative regime.

Despite a wide range of absolute values, the datasets exhibit broadly similar patterns in their summer interannual variability and land-atmospheric coupling relationships. However, regional differences are evident in evapotranspiration and potential evapotranspiration across different datasets, especially in WCE and MED where transitional regimes are dominant. In particular, SiTHv2 and JRA55 exhibit different patterns compared to the other datasets in representing the absolute values of state variables and land–atmosphere coupling. Surface soil moisture exhibits strong agreements across all datasets, showing significant correlations, yet it still displays a wide range of interannual variation and different annual cycles in SiTHv2 and MERRA2.

Analysis of land–atmosphere coupling indicates that northern Europe (energy-limited regime) exhibits stronger atmospheric coupling, while southern Europe (water-limited regime) is dominated by terrestrial coupling; this pattern is well represented across all datasets except JRA55. All datasets consistently capture the large-scale north–south gradient in coupling strength, with weak coupling in northern Europe, strong coupling in southern Europe, and central Europe where evapotranspiration is alternatively controlled by radiation and soil moisture, switching between a wet regime to a transitional one across different years but also within the same season. This spatial structure is in good agreement with previous studies (Seneviratne et al., 2006; Knist et al., 2017). A similar analysis was performed by (Mei and Wang, 2012), who examined land–atmosphere coupling strength over the United States. However, these earlier studies primarily focused on evaluating regional model skill relative to observations, whereas the present study goes beyond this by inter-comparing multiple observational datasets themselves, thereby highlighting the role of observational uncertainty in diagnosing land–atmosphere coupling over Europe.

We conclude that large uncertainties persist in the absolute values of the state variables involved in land-atmosphere coupling processes. However, the interannual variability of such

https://doi.org/10.5194/egusphere-2026-3206
Preprint. Discussion started: 30 June 2026

variables is consistently represented across most of the different observations-based datasets. Some datasets (e.g., JRA55, MERRA2, SiTHv2) exhibit distinct regional time series patterns with partly unplausible features, reflected also in their spatiotemporal coupling characteristics. In general, the representation of land, atmospheric, and combined coupling is comparable across datasets; however, evapotranspiration in JRA55 stands out as a major source of discrepancy, which leads to a misrepresentation of land and atmospheric coupling separately.

https://doi.org/10.5194/egusphere-2026-3206
Preprint. Discussion started: 30 June 2026

Data Availability

All the data are taken from respective open sources and are freely downloadable.

Author contribution:

The study was conceptualized and structured by MS, MD, and SM. All figures were generated, and the first draft of the manuscript was written by MS. MD and SM contributed to improving the writing and provided critical feedback throughout the development of the manuscript.

Competing interest

The authors declare that they have no conflict of interest.

Acknowledgment

The authors gratefully acknowledge all data providers for making their datasets freely available. We sincerely thank Margarida Samso Cabre for downloading the datasets and resolving related issues, which greatly supported this work. MS acknowledges the HPC support provided by BSC, which enabled the data analysis. MS is also grateful to Alvise Aranyossy and Lina Teckentrup for valuable scientific discussions and assistance with the potential evapotranspiration calculations. Special thanks are extended to Charlotte Bohne and Nuria Perez Zanon for their help in improving the manuscript. SM acknowledge the AI4S fellowships within the "Generación D" initiative by Red.es, Ministerio para la Transformación Digital y de la Función Pública of Spain, for talent attraction (C005/24-ED CV1), funded by NextGenerationEU through PRTR. SM and MD acknowledge the Horizon Europe project EXPECT (Grant number

https://doi.org/10.5194/egusphere-2026-3206
Preprint. Discussion started: 30 June 2026

101137656).

Financial support:

This work was supported by the Horizon Europe project CERISE (grant agreement number 101082139), funded by the European Union. Views and opinions expressed are, however, those of the author(s) only and do not necessarily reflect those of the European Union or the Commission. Neither the European Union nor the granting authority can be held responsible for them.

https://doi.org/10.5194/egusphere-2026-3206
Preprint. Discussion started: 30 June 2026

References

Allen, R. G., Pereira, L. S., Raes, D., Smith, M., et al. (1998). Crop evapotranspiration-guidelines for computing crop water requirements-fao irrigation and drainage paper 56. *Fao, Rome*, 300(9):D05109.

Baier, W. and Robertson, G. W. (1965). Estimation of latent evaporation from simple weather observations. *Canadian journal of plant science*, 45(3):276–284.

Bakke, S. J., Ionita, M., and Tallaksen, L. M. (2020). The 2018 northern european hydrological drought and its drivers in a historical perspective. *Hydrology and Earth System Sciences Discussions*, 2020:1–44.

Baret, F., Weiss, M., Lacaze, R., Camacho, F., Makhmara, H., Pacholcyzk, P., and Smets, B. (2013). Geov1: Lai and fapar essential climate variables and fcover global time series capitalizing over existing products. part1: Principles of development and production. *Remote sensing of environment*, 137:299–309.

Barriopedro, D., Fischer, E. M., Luterbacher, J., Trigo, R. M., and García-Herrera, R. (2011). The hot summer of 2010: redrawing the temperature record map of europe. *Science*, 332(6026):220–224.

Beck, H. E., Van Dijk, A. I., Larraondo, P. R., McVicar, T. R., Pan, M., Dutra, E., and Miralles, D. G. (2022). Mswx: global 3-hourly 0.1 bias-corrected meteorological data including near-real-time updates and forecast ensembles. *Bulletin of the American Meteorological Society*, 103(3):E710–E732.

Beillouin, D., Schauberger, B., Bastos, A., Ciais, P., and Makowski, D. (2020). Impact of extreme weather conditions on european crop production in 2018. *Philosophical Transactions of the Royal Society B*, 375(1810):20190510.

Cook, B. I., Smerdon, J. E., Seager, R., and Coats, S. (2014). Global warming and 21 st century drying. *Climate dynamics*, 43:2607–2627.

https://doi.org/10.5194/egusphere-2026-3206
Preprint. Discussion started: 30 June 2026

Cornes, R. C., van der Schrier, G., van den Besselaar, E. J., and Jones, P. D. (2018). An ensemble version of the e-obs temperature and precipitation data sets. *Journal of Geophysical Research: Atmospheres*, 123(17):9391–9409.

Dee, D. P., Uppala, S., Simmons, A. J., Berrisford, P., Poli, P., Kobayashi, S., Andrae, U., Balmaseda, M., Balsamo, G., Bauer, d. P., et al. (2011). The era-interim reanalysis: Configuration and performance of the data assimilation system. *Quarterly Journal of the royal meteorological society*, 137(656):553–597.

Dembélé, M., Ceperley, N., Zwart, S. J., Salvadore, E., Mariethoz, G., and Schaefli, B. (2020). Potential of satellite and reanalysis evaporation datasets for hydrological modelling under various model calibration strategies. *Advances in Water Resources*, 143:103667.

Dirmeyer, P. A. (2006). The hydrologic feedback pathway for land–climate coupling. *Journal of Hydrometeorology*, 7(5):857–867.

Dirmeyer, P. A., Balsamo, G., Blyth, E. M., Morrison, R., and Cooper, H. M. (2021). Land-atmosphere interactions exacerbated the drought and heatwave over northern europe during summer 2018. *AGU Advances*, 2(2):e2020AV000283.

Dirmeyer, P. A. and Halder, S. (2017). Application of the land–atmosphere coupling paradigm to the operational coupled forecast system, version 2 (cfsv2). *Journal of Hydrometeorology*, 18(1):85–108.

Dirmeyer, P. A., Wang, Z., Mbuh, M. J., and Norton, H. E. (2014). Intensified land surface control on boundary layer growth in a changing climate. *Geophysical Research Letters*, 41(4):1290–1294.

Donat, M. G., Pitman, A. J., and Angélil, O. (2018). Understanding and reducing future uncertainty in midlatitude daily heat extremes via land surface feedback constraints. *Geophysical Research Letters*, 45(19):10–627.

Donat, M. G., Pitman, A. J., and Seneviratne, S. I. (2017). Regional warming of hot extremes accelerated by surface energy fluxes. *Geophysical Research Letters*, 44(13):7011–7019.

https://doi.org/10.5194/egusphere-2026-3206
Preprint. Discussion started: 30 June 2026

Dorigo, W., Wagner, W., Albergel, C., Albrecht, F., Balsamo, G., Brocca, L., Chung, D., Ertl, M., Forkel, M., Gruber, A., et al. (2017). Esa cci soil moisture for improved earth system understanding: State-of-the art and future directions. *Remote Sensing of Environment*, 203:185–215.

Dosio, A., Spinoni, J., and Migliavacca, M. (2023). Record-breaking and unprecedented compound hot and dry summers in europe under different emission scenarios. *Environmental Research: Climate*, 2(4):045009.

Ferguson, C. R., Wood, E. F., and Vinukollu, R. K. (2012). A global intercomparison of modeled and observed land–atmosphere coupling. *Journal of Hydrometeorology*, 13(3):749–784.

Fischer, E. M., Seneviratne, S. I., Lüthi, D., and Schär, C. (2007). Contribution of land-atmosphere coupling to recent european summer heat waves. *Geophysical Research Letters*, 34(6).

Gelaro, R., McCarty, W., Suárez, M. J., Todling, R., Molod, A., Takacs, L., Randles, C. A., Darmenov, A., Bosilovich, M. G., Reichle, R., et al. (2017). The modern-era retrospective analysis for research and applications, version 2 (merra-2). *Journal of climate*, 30(14):5419–5454.

Gevaert, A., Miralles, D. G., de Jeu, R. A., Schellekens, J., and Dolman, A. J. (2018). Soil moisture-temperature coupling in a set of land surface models. *Journal of Geophysical Research: Atmospheres*, 123(3):1481–1498.

Gruber, A., Scanlon, T., van der Schalie, R., Wagner, W., and Dorigo, W. (2019). Evolution of the esa cci soil moisture climate data records and their underlying merging methodology. *Earth System Science Data*, 11(2):717–739.

Hargreaves, G. H. and Samani, Z. A. (1982). Estimating potential evapotranspiration. *Journal of the irrigation and Drainage Division*, 108(3):225–230.

https://doi.org/10.5194/egusphere-2026-3206
Preprint. Discussion started: 30 June 2026

Herrera-Lormendez, P., Douville, H., and Matschullat, J. (2023). European summer synoptic circulations and their observed 2022 and projected influence on hot extremes and dry spells. *Geophysical Research Letters*, 50(18):e2023GL104580.

Hersbach, H., Bell, B., Berrisford, P., Hirahara, S., Horányi, A., Muñoz-Sabater, J., Nicolas, J., Peubey, C., Radu, R., Schepers, D., et al. (2020). The era5 global reanalysis. *Quarterly Journal of the Royal Meteorological Society*, 146(730):1999–2049.

Hirsch, A., Pitman, A., Seneviratne, S. I., Evans, J., and Haverd, V. (2014). Summertime maximum and minimum temperature coupling asymmetry over australia determined using wrf. *Geophysical Research Letters*, 41(5):1546–1552.

Hirschi, M., Seneviratne, S. I., Alexandrov, V., Boberg, F., Boroneant, C., Christensen, O. B., Formayer, H., Orlowsky, B., and Stepanek, P. (2011). Observational evidence for soil-moisture impact on hot extremes in southeastern europe. *Nature Geoscience*, 4(1):17–21.

Hoy, A., Hänsel, S., Skalak, P., Ustrnul, Z., and Bochníček, O. (2017). The extreme european summer of 2015 in a long-term perspective. *International Journal of Climatology*, 37(2):943–962.

Iturbide, M., Gutiérrez, J. M., Alves, L. M., Bedia, J., Cerezo-Mota, R., Cimadevilla, E., Cofiño, A. S., Di Luca, A., Faria, S. H., Gorodetskaya, I. V., et al. (2020). An update of ipcc climate reference regions for subcontinental analysis of climate model data: definition and aggregated datasets. *Earth System Science Data*, 12(4):2959–2970.

Jung, M., Koirala, S., Weber, U., Ichii, K., Gans, F., Camps-Valls, G., Papale, D., Schwalm, C., Tramontana, G., and Reichstein, M. (2019). The fluxcom ensemble of global land-atmosphere energy fluxes. *Scientific data*, 6(1):74.

Kew, S. f., Philip, S. Y., Van Oldenborgh, G. J., van der Schrier, G., Otto, F. E., and Vautard, R. (2019). The exceptional summer heat wave in southern europe 2017. *Bulletin of the American Meteorological Society*, 100:S49–S53.

https://doi.org/10.5194/egusphere-2026-3206
Preprint. Discussion started: 30 June 2026

Kim, H., Parinussa, R., Konings, A. G., Wagner, W., Cosh, M. H., Lakshmi, V., Zohaib, M., and Choi, M. (2018). Global-scale assessment and combination of smap with ascat (active) and amsr2 (passive) soil moisture products. *Remote Sensing of Environment*, 204:260–275.

Klein, T. A., Wijngaard, J., Können, G., Van Engelen, A., Böhm, R., Demarée, G., Gocheva, A., Mileta, M., Pashiardis, S., Hejkrlik, L., et al. (2002). Daily dataset of 20th-century surface air temperature and precipitation series for the european climate assessment. *International Journal of Climatology*, 22(12):1441–1453.

Knist, S., Goergen, K., Buonomo, E., Christensen, O. B., Colette, A., Cardoso, R. M., Fealy, R., Fernández, J., García-Díez, M., Jacob, D., et al. (2017). Land-atmosphere coupling in euro-cordex evaluation experiments. *Journal of Geophysical Research: Atmospheres*, 122(1):79–103.

Kobayashi, S., Ota, Y., Harada, Y., Ebita, A., Moriya, M., Onoda, H., Onogi, K., Kamahori, H., Kobayashi, C., Endo, H., et al. (2015). The jra-55 reanalysis: General specifications and basic characteristics. *Journal of the Meteorological Society of Japan. Ser. II*, 93(1):5–48.

Koster, R. D., Sud, Y., Guo, Z., Dirmeyer, P. A., Bonan, G., Oleson, K. W., Chan, E., Verseghy, D., Cox, P., Davies, H., et al. (2006). Glace: the global land–atmosphere coupling experiment. part i: overview. *Journal of Hydrometeorology*, 7(4):590–610.

Lebedeva, M. G., Krymskaya, O. V., Lupo, A. R., Chendev, Y. G., Petin, A. N., and Solovyov, A. B. (2016). Trends in summer season climate for eastern europe and southern russia in the early 21st century. *Advances in meteorology*, 2016(1):5035086.

Lhotka, O. and Kyselỳ, J. (2015). Hot central-european summer of 2013 in a long-term context. *International Journal of Climatology*, 35(14).

Li, M., Wu, P., and Ma, Z. (2020). A comprehensive evaluation of soil moisture and soil temperature from third-generation atmospheric and land reanalysis data sets. *Int. J. Climatol*, 40(13):5744–5766.

https://doi.org/10.5194/egusphere-2026-3206
Preprint. Discussion started: 30 June 2026

Li, Y., Qin, Y., and Rong, P. (2022). Evolution of potential evapotranspiration and its sensitivity to climate change based on the thornthwaite, hargreaves, and penman–monteith equation in environmental sensitive areas of china. *Atmospheric Research*, 273:106178.

Liang, S., Cheng, J., Jia, K., Jiang, B., Liu, Q., Xiao, Z., Yao, Y., Yuan, W., Zhang, X., Zhao, X., et al. (2021). The global land surface satellite (glass) product suite. *Bulletin of the American Meteorological Society*, 102(2):E323–E337.

Logan, T., Bourgault, P., Smith, T., Huard, D., Biner, S., Labonté, M., Rondeau-Genesse, G., Fyke, J., Aoun, A., Roy, P., et al. (2022). Ouranosinc/xclim: v0. 31.0. *CERN: Meyrin, Switzerland*.

Lorenz, R., Jaeger, E. B., and Seneviratne, S. I. (2010). Persistence of heat waves and its link to soil moisture memory. *Geophysical Research Letters*, 37(9).

Martens, B., Miralles, D. G., Lievens, H., Van Der Schalie, R., De Jeu, R. A., Fernández-Prieto, D., Beck, H. E., Dorigo, W. A., and Verhoest, N. E. (2017). Gleam v3: Satellite-based land evaporation and root-zone soil moisture. *Geoscientific Model Development*, 10(5):1903–1925.

Materia, S., Ardilouze, C., Prodhomme, C., Donat, M. G., Benassi, M., Doblas-Reyes, F. J., Peano, D., Caron, L.-P., Ruggieri, P., and Gualdi, S. (2022). Summer temperature response to extreme soil water conditions in the mediterranean transitional climate regime. *Climate Dynamics*, 58(7):1943–1963.

Mei, R. and Wang, G. (2012). Summer land–atmosphere coupling strength in the united states: Comparison among observations, reanalysis data, and numerical models. *Journal of Hydrometeorology*, 13(3):1010–1022.

Miralles, D. G., Gentine, P., Seneviratne, S. I., and Teuling, A. J. (2019). Land–atmospheric feedbacks during droughts and heatwaves: state of the science and current challenges. *Annals of the New York Academy of Sciences*, 1436(1):19–35.

https://doi.org/10.5194/egusphere-2026-3206
Preprint. Discussion started: 30 June 2026

679 Miralles, D. G., Holmes, T., De Jeu, R., Gash, J., Meesters, A., and Dolman, A. (2011). Global
680 land-surface evaporation estimated from satellite-based observations. *Hydrology and Earth*
681 *System Sciences*, 15(2):453–469.

682 Miralles, D. G., Teuling, A. J., Van Heerwaarden, C. C., and Vilà-Guerau de Arellano, J. (2014).
683 Mega-heatwave temperatures due to combined soil desiccation and atmospheric heat accu-
684 mulation. *Nature geoscience*, 7(5):345–349.

685 Moratiel, R., Bravo, R., Saa, A., Tarquis, A. M., and Almorox, J. (2020). Estimation of evap-
686 otranspiration by the food and agricultural organization of the united nations (fao) penman–
687 monteith temperature (pmt) and hargreaves–samani (hs) models under temporal and spatial
688 criteria–a case study in duero basin (spain). *Natural Hazards and Earth System Sciences*,
689 20(3):859–875.

690 Mousa, B. and Shu, H. (2020). Spatial evaluation and assimilation of smap, smos, and ascat
691 satellite soil moisture products over africa using statistical techniques. *Earth and Space*
692 *Science*, 7(1):e2019EA000841.

693 Mueller, B. and Seneviratne, S. I. (2012). Hot days induced by precipitation deficits at the
694 global scale. *Proceedings of the national academy of sciences*, 109(31):12398–12403.

695 Muñoz-Sabater, J., Dutra, E., Agustí-Panareda, A., Albergel, C., Arduini, G., Balsamo, G.,
696 Boussetta, S., Choulga, M., Harrigan, S., Hersbach, H., et al. (2021). Era5-land: A
697 state-of-the-art global reanalysis dataset for land applications. *Earth system science data*,
698 13(9):4349–4383.

699 Nguyen, H. H., Kim, H., and Choi, M. (2017). Evaluation of the soil water content using
700 cosmic-ray neutron probe in a heterogeneous monsoon climate-dominated region. *Advances*
701 *in Water Resources*, 108:125–138.

702 Orth, R., Zscheischler, J., and Seneviratne, S. I. (2016). Record dry summer in 2015 challenges
703 precipitation projections in central europe. *Scientific reports*, 6(1):28334.

https://doi.org/10.5194/egusphere-2026-3206
Preprint. Discussion started: 30 June 2026

Philip, S. Y., Kew, S. F., Hauser, M., Guillod, B. P., Teuling, A. J., Whan, K., Uhe, P., and Oldenborgh, G. J. v. (2018). Western us high june 2015 temperatures and their relation to global warming and soil moisture. *Climate Dynamics*, 50(7):2587–2601.

Preimesberger, W., Scanlon, T., Su, C.-H., Gruber, A., and Dorigo, W. (2020). Homogenization of structural breaks in the global esa cci soil moisture multisatellite climate data record. *IEEE Transactions on Geoscience and Remote Sensing*, 59(4):2845–2862.

Preimesberger, W., Stradiotti, P., and Dorigo, W. (2025). Esa cci soil moisture gapfilled: an independent global gap-free satellite climate data record with uncertainty estimates. *Earth System Science Data*, 17(9):4305–4329.

Priestley, C. H. B. and Taylor, R. J. (1972). On the assessment of surface heat flux and evaporation using large-scale parameters. *Monthly weather review*, 100(2):81–92.

Quesada, B., Vautard, R., Yiou, P., Hirschi, M., and Seneviratne, S. I. (2012). Asymmetric european summer heat predictability from wet and dry southern winters and springs. *Nature Climate Change*, 2(10):736–741.

Ratna, S. B., Ratnam, J., Behera, S. K., Cherchi, A., Wang, W., and Yamagata, T. (2017). The unusual wet summer (july) of 2014 in southern europe. *Atmospheric Research*, 189:61–68.

Rebetez, M., Mayer, H., Dupont, O., Schindler, D., Gartner, K., Kropp, J. P., and Menzel, A. (2006). Heat and drought 2003 in europe: a climate synthesis. *Annals of Forest Science*, 63(6):569–577.

Rousi, E., Fink, A. H., Andersen, L. S., Becker, F. N., Beobide-Arsuaga, G., Breil, M., Cozzi, G., Heinke, J., Jach, L., Niermann, D., et al. (2023). The extremely hot and dry 2018 summer in central and northern europe from a multi-faceted weather and climate perspective. *Natural Hazards and Earth System Sciences*, 23(5):1699–1718.

Santanello Jr, J. A., Peters-Lidard, C. D., and Kumar, S. V. (2011). Diagnosing the sensitivity of local land–atmosphere coupling via the soil moisture–boundary layer interaction. *Journal of Hydrometeorology*, 12(5):766–786.

https://doi.org/10.5194/egusphere-2026-3206
Preprint. Discussion started: 30 June 2026

730 Schwitalla, T., Jach, L., Wulfmeyer, V., and Warrach-Sagi, K. (2025). Soil moisture–
731 atmosphere coupling strength over central europe in the recent warming climate. *Natural*
732 *Hazards and Earth System Sciences*, 25(4):1405–1424.

733 Seneviratne, S. I., Corti, T., Davin, E. L., Hirschi, M., Jaeger, E. B., Lehner, I., Orlowsky, B.,
734 and Teuling, A. J. (2010). Investigating soil moisture–climate interactions in a changing
735 climate: A review. *Earth-Science Reviews*, 99(3-4):125–161.

736 Seneviratne, S. I., Lüthi, D., Litschi, M., and Schär, C. (2006). Land–atmosphere coupling and
737 climate change in europe. *Nature*, 443(7108):205–209.

738 Seo, Y.-W. and Ha, K.-J. (2022). Changes in land-atmosphere coupling increase compound
739 drought and heatwaves over northern east asia. *Npj Climate and Atmospheric Science*,
740 5(1):100.

741 Sherwood, S. and Fu, Q. (2014). A drier future? *Science*, 343(6172):737–739.

742 Thorne, P. and Vose, R. (2010). Reanalyses suitable for characterizing long-term trends. *Bul-*
743 *letin of the American Meteorological Society*, 91(3):353–362.

744 Thornthwaite, C. W. (1948). An approach toward a rational classification of climate. *Geo-*
745 *graphical review*, 38(1):55–94.

746 Trajkovic, S. (2007). Hargreaves versus penman-monteith under humid conditions. *Journal of*
747 *Irrigation and Drainage Engineering*, 133(1):38–42.

748 Tran, B. N., Van Der Kwast, J., Seyoum, S., Uijlenhoet, R., Jewitt, G., and Mul, M. (2023). Un-
749 certainty assessment of satellite remote-sensing-based evapotranspiration estimates: a sys-
750 tematic review of methods and gaps. *Hydrology and Earth System Sciences*, 27(24):4505–
751 4528.

752 Trenberth, K. E., Fasullo, J. T., and Kiehl, J. (2009). Earth's global energy budget. *Bulletin of*
753 *the american meteorological society*, 90(3):311–324.

https://doi.org/10.5194/egusphere-2026-3206
Preprint. Discussion started: 30 June 2026

Vautard, R., Yiou, P., D'andrea, F., De Noblet, N., Viovy, N., Cassou, C., Polcher, J., Ciais, P., Kageyama, M., and Fan, Y. (2007). Summertime european heat and drought waves induced by wintertime mediterranean rainfall deficit. *Geophysical Research Letters*, 34(7).

Wieder, W., Boehnert, J., Bonan, G., and Langseth, M. (2014). Regridded harmonized world soil database v1. 2. *ORNL DAAC*.

Wilcox, L. J., Yiou, P., Hauser, M., Lott, F. C., van Oldenborgh, G. J., Colfescu, I., Dong, B., Hegerl, G., Shaffrey, L., and Sutton, R. (2018). Multiple perspectives on the attribution of the extreme european summer of 2012 to climate change. *Climate Dynamics*, 50(9):3537–3555.

Winkler, K., Fuchs, R., Rounsevell, M., and Herold, M. (2021). Global land use changes are four times greater than previously estimated. *Nature communications*, 12(1):2501.

Wu, Z., Feng, H., He, H., Zhou, J., and Zhang, Y. (2021). Evaluation of soil moisture climatology and anomaly components derived from era5-land and gldas-2.1 in china. *Water Resources Management*, 35:629–643.

Xu, C., Wang, W., Hu, Y., and Liu, Y. (2024). Evaluation of era5, era5-land, gldas-2.1, and gleam potential evapotranspiration data over mainland china. *Journal of Hydrology: Regional Studies*, 51:101651.

Yi, K., Senay, G. B., Fisher, J. B., Wang, L., Suvočarev, K., Chu, H., Moore, G. W., Novick, K. A., Barnes, M. L., Keenan, T. F., et al. (2024). Challenges and future directions in quantifying terrestrial evapotranspiration. *Water Resources Research*, 60(10):e2024WR037622.

Zhang, K., Chen, H., Ma, N., Shang, S., Wang, Y., Xu, Q., and Zhu, G. (2024). A global dataset of terrestrial evapotranspiration and soil moisture dynamics from 1982 to 2020. *Scientific Data*, 11(1):445.

Zheng, C., Jia, L., and Zhao, T. (2023). A 21-year dataset (2000–2020) of gap-free global daily surface soil moisture at 1-km grid resolution. *Scientific Data*, 10(1):139.

https://doi.org/10.5194/egusphere-2026-3206
Preprint. Discussion started: 30 June 2026

778 Zhuo, L., Han, D., Dai, Q., Islam, T., and Srivastava, P. K. (2015). Appraisal of nldas-2 multi-
779 model simulated soil moistures for hydrological modelling. *Water Resources Management*,
780 29:3503–3517.

https://doi.org/10.5194/egusphere-2026-3206
Preprint. Discussion started: 30 June 2026

Appendix A

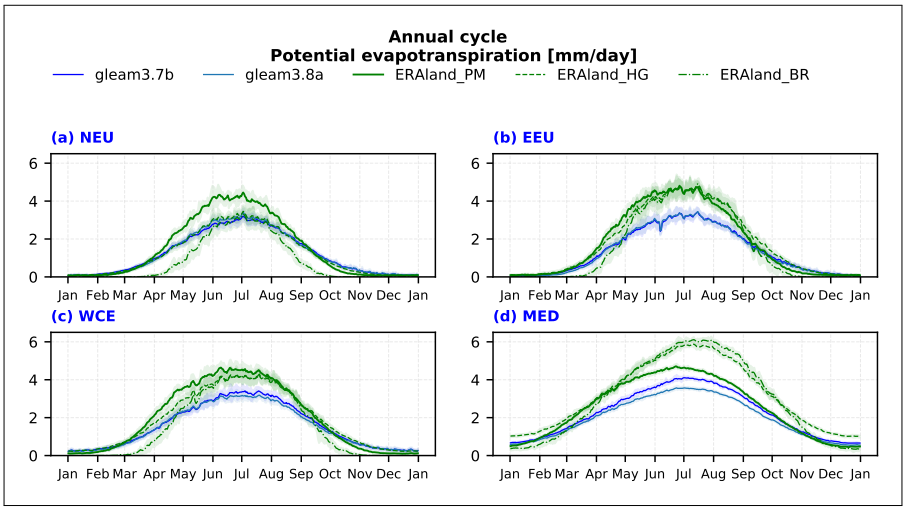

Figure A1: Annual cycle of PET for NEU, EEU, WCE, and MED. For GLEAM datasets, we used the provided variable, which is shown in solid lines. Penman-Monteith method is shown as solid lines, Hargreaves method as dashed lines, Baier's method as dotted dashed lines, and Thornthwaite's method as dotted lines.

https://doi.org/10.5194/egusphere-2026-3206
Preprint. Discussion started: 30 June 2026

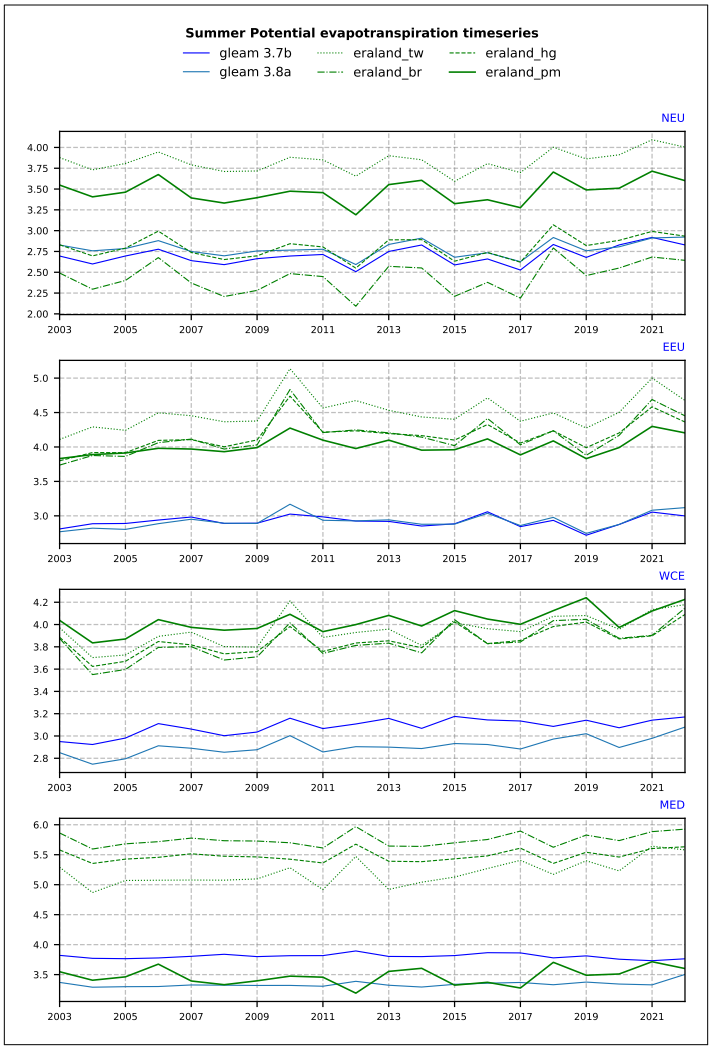

Figure A2: Interannual variation of PET for NEU, EEU, WCE, and MED. For GLEAM datasets, as we used the provided variable, which is shown in solid lines. Penman-Monteith method is shown as solid lines, Hargreaves method as dashed lines, Baier's method as dotted dashed lines, and Thornthwaite's method as dotted lines.

https://doi.org/10.5194/egusphere-2026-3206
Preprint. Discussion started: 30 June 2026

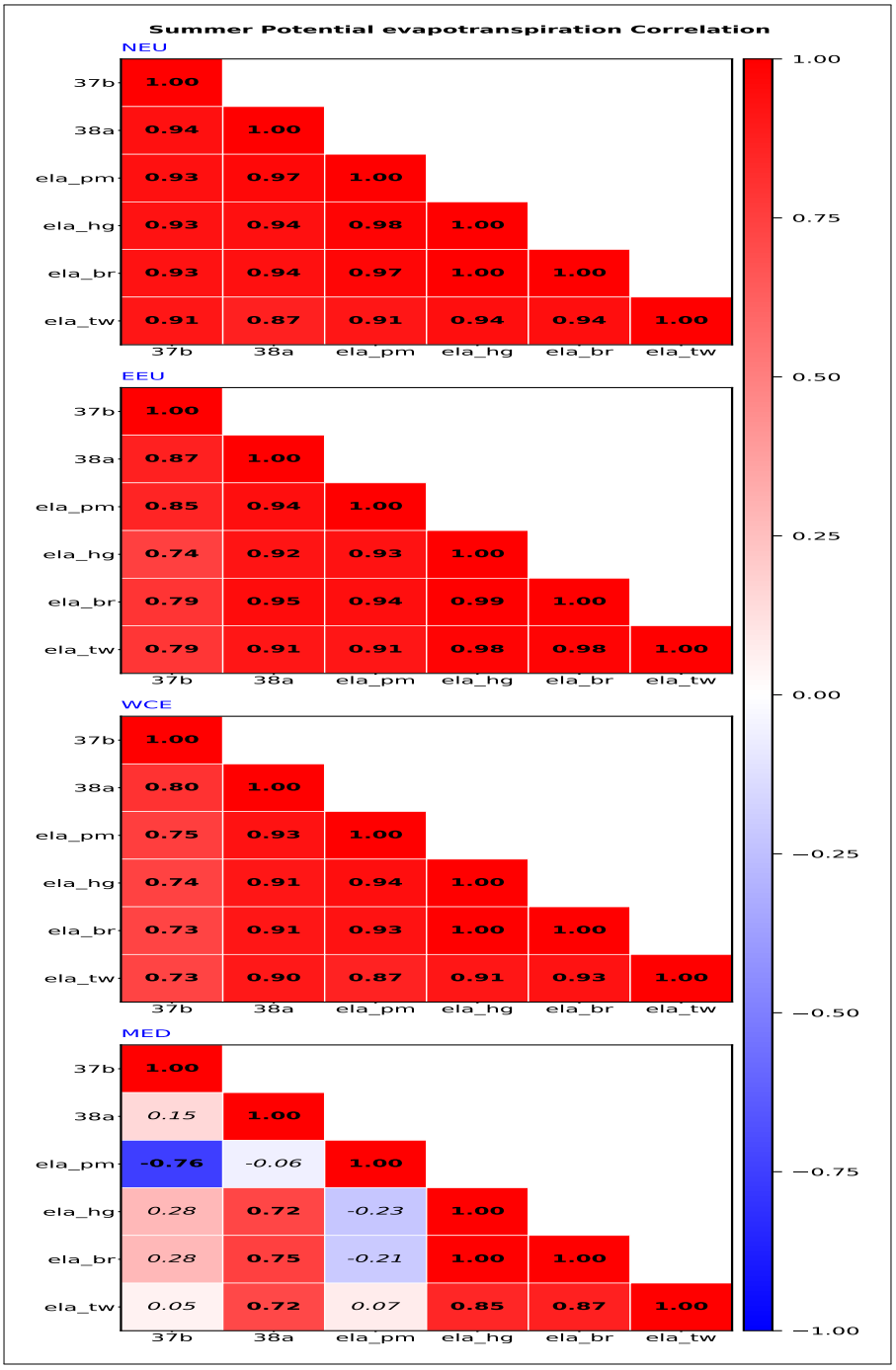

Figure A3: correlation matrices of PET for NEU, EEU, WCE, and MED, including all datasets and all different methods used in this study.